Radiative recombination and optical gain spectra in biaxially strained *n*-type germanium

M. Virgilio,[1,2,*] C. L. Manganelli,[1,2] G. Grosso,[1,2] G. Pizzi,[3] and G. Capellini[4,5]

[1]*Dipartimento di Fisica "E. Fermi," Università di Pisa, Largo Pontecorvo 3, I-56127 Pisa, Italy*

[2]*NEST, Istituto Nanoscienze-CNR, Piazza San Silvestro 12, I-56127 Pisa, Italy*

[3]*Theory and Simulation of Materials, École Polytechnique Fédérale de Lausanne, Station 12, CH-1015 Lausanne, Switzerland*

[4]*Dipartimento di Scienze, Università degli studi Roma Tre, Viale Marconi 446, I-00146 Roma, Italy*

[5]*IHP, Im Technologiepark 25, 15236 Frankfurt (Oder), Germany*

(Received 4 March 2013; revised manuscript received 18 April 2013; published 21 June 2013)

We calculate band-to-band radiative transition rate spectra in pure Ge as functions of applied tensile strain, heavy doping, charge injection density, and temperature. Direct and indirect phonon-assisted transitions are considered. Deformation potential theory is adopted to describe the conduction and valence near-gap edges. Biaxial strain has required appropriate treatment of system anisotropy through the evaluation of the mass tensor components for the different bands involved in the studied transitions. Population distribution in the Γ and L conduction valleys and in the valence states near Γ have been evaluated accordingly considering the degeneracy condition of the sample, induced by high doping and high injection charge density. Also the effect of strain on the dipole matrix elements have been properly taken into account. The energy-resolved near-infrared spontaneous recombination spectra and the TE and TM polarized absorption/gain spectra have been obtained for a broad range of n-type doping, strain values, and excitation densities. We conclude that, despite the free carrier losses, net gain values as high as 6000 cm^{-1}, are achievable for doping density and strain values reported in the literature.

DOI: 10.1103/PhysRevB.87.235313 PACS number(s): 78.20.Ci, 78.20.Bh, 78.55.Ap

I. INTRODUCTION

Over the past few years, silicon photonics has demonstrated its potential as a solution for realizing high-performance electro-optic devices. Numerous research institutes have reported the integration of electro-optic modulators, photodetectors, and advanced passive optical devices such as wavelength filters and coupling structures, with device performances that are in many cases on par or better than those of their III-V semiconductor-based counterparts typically used in high-end telecom systems.[1–3] The only missing piece in the Si-photonics toolkit is an efficient, monolithically integrated light source.[1] Ge is considered the best material candidate to solve this problem owing to its compatibility with silicon and to its peculiar band structure in which, unlike silicon, the indirect band-gap minimum at the L point is relatively close to the direct band gap minimum at the Γ point. This energy difference can be further reduced applying a biaxial tensile strain to Ge (Ref. 4). Relying on this phenomenon, Michel and co-workers have recently demonstrated the operation of both optically[5,6] and electrically[7] pumped integrated laser based on highly n-type doped and tensile-strained Ge, integrated on Si via a complementary metal-oxide semiconductor-compatible approach. Although this has to be considered a ground-breaking result, the demonstrated device is doomed by very high threshold current, which is unacceptable in an integrated platform, and moderate efficiency. As recently pointed out,[8] this is due to the modest applied strain ($\sim$0.2%) that requires a high doping level ($\sim 10^{20}$ cm^{-3}) for the realization of population inversion. The high density of carriers, on the other hand, induces high free carrier absorption, decreasing the net optical gain of the material. For the further development of tensile Ge-based lasers it is therefore of paramount importance to investigate the effect of both strain and doping on the Ge optical properties. Numerical studies in the recent literature have addressed this problem without deep analysis of the numerous effects due to the system anisotropy induced by the strain. The lacking of such information, together with the demonstrated possibility to reach values of strain in the percent range,[9] motivate a more detailed theoretical investigation of the optical properties of tensile and doped Ge, which is the object of the present paper.

In this work we calculate the recombination and absorption/gain energy-resolved spectra for bulk Ge in realistic conditions of strain, doping, charge injection, and temperature. Both direct and indirect phonon assisted radiative processes are here considered. The intraband contribution to the absorption spectrum due to the presence of free carrier in the valence and conduction bands is also discussed. This approach allows us to evaluate the energy-resolved spectrum of the above quantities as a function of strain, doping, and temperature. In our model strain effects on the band edges are considered within the deformation potential theory; moreover, we take into account also the strain influence on the band curvatures, population distributions, and the dipole matrix elements. Dipole matrix elements have been calculated by means of an atomistic model so that also strain-dependent selection rules for the TE and TM polarized transitions are properly derived.

The paper is organized as follows. In Sec. II we describe the adopted model for the evaluation of the direct and phonon-assisted contributions to the optical recombination rate and to the absorption spectra. Effects due to free carrier absorption of light are also evaluated. In Sec. III we report and discuss numerical results for the recombination and absorption spectra, obtained as a function of different values of the tensile strain field, doping concentrations, and temperature, and for different excitation densities. Conclusions are given in Sec. IV.

 ©2013 American Physical Society

II. MODEL DESCRIPTION

A. Band edges and effective masses

In order to model the steady-state radiative recombinations in biaxially strained [001] Ge films, we first evaluate the effect of lattice strain on the near-gap valence and conduction bands. In particular, we calculate the band-edge energies and the values of the corresponding effective masses. If we set the zero of the energy scale at the barycenter of heavy-hole (HH), light-hole (LH), and split-off (SO) valence bands, the Γ_c- and L_c-point conduction edges are located at[10]

$$E^{L_c,\Gamma_c} = \tfrac{1}{3}\Delta_{\mathrm{so}} + E_g^{L,\Gamma} + \Delta E_h^{L,\Gamma}, \tag{1}$$

where E_g^L and E_g^Γ are, respectively, the fundamental indirect and direct gaps of unstrained bulk Ge, and Δ_{so} is the spin-orbit interaction parameter. The $\Delta E_h^{L,\Gamma}$ terms represent the modification of the Ge gaps due to the hydrostatic component of the strain field (the uniaxial component of the strain tensor does not affect the L- and Γ-point conduction band edges) and are evaluated according to the expression

$$\Delta E_h^{L,\Gamma} = \left(a_c^{L,\Gamma} - a_v\right)(2\varepsilon_\parallel + \varepsilon_\perp), \tag{2}$$

where $\varepsilon_\parallel$ and $\varepsilon_\perp$ are the in-plane and perpendicular components of the strain tensor referred to the [001] growth direction. The in-plane (positive) strain component $\varepsilon_\parallel$ is due to the matching of the lattice constant along the parallel direction of the strained Ge layer with an appropriate relaxed substrate. The perpendicular strain component $\varepsilon_\perp$ is a function of $\varepsilon_\parallel$ and can be calculated by minimization of the Ge elastic energy. In Eq. (2) $a_c^{L,\Gamma}$ and a_v are the deformation potentials for the L and Γ conduction edges and for the barycenter of the valence bands, respectively; their values are reported in Table I together with other relevant material parameters used in the model. The temperature dependence of the direct and indirect gaps $E_g^{L,\Gamma}$ is calculated exploiting the relation[11,12]

$$E_g^{L,\Gamma}(T) = E_g^{L,\Gamma}(0) - T^2\frac{\alpha^{L,\Gamma}}{T+\beta^{L,\Gamma}}. \tag{3}$$

Finally, the energies of the edges of the valence bands are given by[10]

$$\begin{aligned}
E^{\mathrm{HH}} &= \frac{1}{3}\Delta_{\mathrm{so}} - \frac{\delta E}{2},\\
E^{\mathrm{LH}} &= -\frac{1}{6}\Delta_{\mathrm{so}} + \frac{\delta E}{4} + \frac{\sqrt{\Delta_{\mathrm{so}}^2 + \Delta_{\mathrm{so}}\delta E + \frac{9}{4}\delta E^2}}{2},\\
E^{\mathrm{SO}} &= -\frac{1}{6}\Delta_{\mathrm{so}} + \frac{\delta E}{4} - \frac{\sqrt{\Delta_{\mathrm{so}}^2 + \Delta_{\mathrm{so}}\delta E + \frac{9}{4}\delta E^2}}{2},\\
\delta E &= 2b(\varepsilon_\perp - \varepsilon_\parallel),
\end{aligned} \tag{4}$$

where b is the tetragonal deformation potential for the valence bands (see Table I).

The strain field affects also the band curvature of the near-edge valence bands and thus impacts the effective masses. To take this into account we distinguish between band dispersion along the in-plane and the perpendicular directions, relying on the following expressions for the HH, LH, and SO effective valence masses[13]:

$$\begin{aligned}
m_\parallel^{\mathrm{HH}} &= \frac{m_0}{\gamma_1+\gamma_2}, \quad m_\perp^{\mathrm{HH}} = \frac{m_0}{\gamma_1 - 2\gamma_2},\\
m_\parallel^{\mathrm{LH}} &= \frac{m_0}{\gamma_1 - f_+\gamma_2}, \quad m_\perp^{\mathrm{LH}} = \frac{m_0}{\gamma_1 + 2f_+\gamma_2},\\
m_\perp^{\mathrm{SO}} &= \frac{m_0}{\gamma_1 + 2f_-\gamma_2}, \quad m_\parallel^{\mathrm{SO}} = \frac{m_0}{\gamma_1 - f_-\gamma_2},
\end{aligned} \tag{5}$$

where $\gamma_{1,2}$ are the Luttinger parameters and $f_\pm$ is an anisotropy parameter that depends on the uniaxial component of the strain tensor; its explicit expression is reported in Ref. 13. For what concerns the conduction bands, we neglect the influence of the strain field on the (isotropic) Γ-point effective mass, due to the absence of appropriate data in the literature; on the other hand, strain-dependent values for the longitudinal ($m_l^{L_c}$) and transverse ($m_t^{L_c}$) L-point effective masses are included in the model relying on the parametrization derived in Ref. 14. The density-of-states masses associated with the lowest conduction edge at L and to the valence edges Γ_v =HH, LH, SO are given by

$$m^{*L_c} = \left(m_l^{L_c} m_t^{L_c} m_t^{L_c}\right)^{\frac{1}{3}}, \quad m^{*\Gamma_v} = \left(m_\perp^{\Gamma_v} m_\parallel^{\Gamma_v} m_\parallel^{\Gamma_v}\right)^{\frac{1}{3}}. \tag{6}$$

Finally, to evaluate recombination and gain spectra related to optical transitions occurring between the Γ_c and the HH, LH, and SO states, it is useful to introduce also the direction-dependent reduced masses $m_{\parallel,\perp}^{\Gamma_{vc}}$ defined by

$$\frac{1}{m_{\parallel,\perp}^{\Gamma_{vc}}} = \frac{1}{m_{\parallel,\perp}^{\Gamma_v}} + \frac{1}{m^{\Gamma_c}}. \tag{7}$$

We conclude this section with some remarks about the parabolic approximation adopted in our model. As a matter of fact, due to the very high density of carriers present in the investigated systems, one might conclude that the parabolic approximation adopted here is not appropriate, in particular for the description of the valence bands. However, this is not the case owing to the fact that the large majority of the electrons populates the conduction L_c valleys (see Fig. 2), which, in a large energy range, is well described by a quadratic dispersion. Furthermore, the higher energy Γ_c valley has large curvature. It follows that in a neighborhood of the Γ point the active direct recombination transitions are characterized by small values of $\boldsymbol{k}$. Since the spectra are generally dominated by these transitions, the deviation from the parabolic dispersion of the valence bands in this small momentum region can be

TABLE I. Values for the material parameters used in the model and related references.

Parameter	Value	Ref.	Parameter	Value	Ref.
E_g^Γ (low T)	889 meV	23	$a_c^L - a_v$	−2.78 eV	10
E_g^L (low T)	744 meV	23	b	−1.88 eV	4
α^Γ	−0.684 meV/K	11	m^{Γ_c}	$0.038m_0$	23
α^L	−0.48 meV/K	12	γ_1	13.25	23
β^Γ	398 K	11	γ_2	4.20	23
β^L	235 K	12	n_1	4.00	23
Δ_{so}	0.296 eV	24	ρ	5.323 g/cm^3	23
C_{11}/C_{12}	2.662	23	D_{eff}	2 eV/Å	25
$a_c^\Gamma - a_v$	−10.06 eV	26	$\hbar\omega_{\mathrm{eff}}$	27.56 meV	25

safely neglected in the determination of the optical properties. To validate these assumptions, we have compared in selected cases the spontaneous recombination rate spectra obtained by the tight-binding Hamiltonian model of Refs. 15 and 16, which gives the correct band dispersion in the whole Brillouin zone, with those obtained by means of the present parabolic $\boldsymbol{k}\cdot\boldsymbol{p}$ model, finding very good agreement.

B. Spontaneous radiative recombination rate

To calculate the spontaneous radiative recombination and the gain coefficient, we consider direct ($\Gamma_c \to \Gamma_v$) and indirect ($L_c \to \Gamma_v$) optical transitions and include contributions from all three valence bands. The above quantities are here calculated under the condition of spatially uniform distribution of the excess photogenerated carriers and charge neutrality. With the above assumptions the spontaneous radiative recombination and the absorption coefficient are spatially independent quantities controlled by the value of the quasi-Fermi levels in the valence and conduction bands. In our simulations the quasi-Fermi energies are calculated self-consistently to obtain the input value of the excess carrier density.

The strain field affects the value of the dipole matrix element $p^{\Gamma_{vc}}$ between a given valence state in the band Γ_v and a conduction state in the band Γ_c through the modification of the orbital composition of the involved levels. This effect is considered exploiting a tight-binding model[15,16] to determine the strain-dependent values of $p^{\Gamma_{vc}}$. Moreover, in the evaluation of the recombination rate and absorption coefficient spectra the reduction of the symmetry of the system caused by the biaxial strain field is fully considered. Their explicit expressions are reported in the following.

The radiative spontaneous recombination rate per unit of energy due to direct transitions $R^{\Gamma_c\Gamma_v}(\hbar\omega)$ is given by[17]

$$R^{\Gamma_c\Gamma_v}(\hbar\omega) = \frac{n_1 e^2\omega|p^{\Gamma_{vc}}|^2}{6\pi^3\varepsilon_0 m_0^2\hbar c^3} \times \int_{-\infty}^{\infty} dk_\perp \int_0^{\infty} k_\parallel dk_\parallel \delta\left(E_{\boldsymbol{k}}^{\Gamma_c} - E_{\boldsymbol{k}}^{\Gamma_v} - \hbar\omega\right) \times f_e\left(E_{\boldsymbol{k}}^{\Gamma_c}\right) f_h\left(E_{\boldsymbol{k}}^{\Gamma_v}\right), \tag{8}$$

where the $\boldsymbol{k}$ dependence near the band edges of $p^{\Gamma_{vc}}$ has been neglected, n_1 is the real part of the refractive index, $f_{e,h}$ are Fermi distributions for the electrons and holes, evaluated exploiting the self-consistent determination of the conduction and valence quasi-Fermi levels, and the band curvatures are described in cylindrical approximation by

$$E_{\boldsymbol{k}}^{\Gamma_c} = E^{\Gamma_c} + \frac{\hbar^2 k^2}{2m^{\Gamma_c}}, \qquad E_{\boldsymbol{k}}^{\Gamma_v} = E^{\Gamma_v} - \frac{\hbar^2 k_\parallel^2}{2m_\parallel^{\Gamma_v}} - \frac{\hbar^2 k_\perp^2}{2m_\perp^{\Gamma_v}}. \tag{9}$$

Note that from the above equations it follows that no one-to-one correspondence exists between the modulus of the $\boldsymbol{k}$ vector and the photon energy, differently from what happens when isotropic dispersion in both the conduction and the valence bands is assumed. After integration over the $k_\parallel$ variable, expression (8) becomes

$$R^{\Gamma_c\Gamma_v}(\hbar\omega) = \frac{n_1 e^2\omega m_\parallel^{\Gamma_{vc}}|p^{\Gamma_{vc}}|^2}{3\pi^3\varepsilon_0 m_0^2\hbar^3 c^3} \times \int_0^{k^{\mathrm{dir}}} dk_\perp \frac{1}{\left(1+e^{\frac{Ak_\perp^2+B^c}{kT}}\right)\left(1+e^{\frac{-Ak_\perp^2-B^v}{kT}}\right)}, \tag{10}$$

where we have defined

$$A = \frac{\hbar^2}{2}\left(\frac{m_\parallel^{\Gamma_{vc}}}{m_\parallel^{\Gamma_v} m_\perp^{\Gamma_{vc}}} - \frac{1}{m_\perp^{\Gamma_v}}\right),$$
$$B^v = E^{\Gamma_v} - \frac{m_\parallel^{\Gamma_{vc}}}{m_\parallel^{\Gamma_v}}[\hbar\omega - (E^{\Gamma_c} - E^{\Gamma_v})] - E_h^F,$$
$$B^c = E^{\Gamma_c} + \frac{m_\parallel^{\Gamma_{vc}}}{m^{\Gamma_c}}[\hbar\omega - (E^{\Gamma_c} - E^{\Gamma_v})] - E_e^F,$$
$$k^{\mathrm{dir}} = \sqrt{\frac{2m_\perp^{\Gamma_{vc}}}{\hbar^2}[\hbar\omega - (E^{\Gamma_c} - E^{\Gamma_v})]}, \tag{11}$$

and $m_{\parallel,\perp}^{\Gamma_{vc}}$ are the reduced masses defined in Eq. (7), and $E_{e,h}^F$ are the quasi-Fermi energies for electrons and holes.

The contribution to the spontaneous radiative recombination rate related to phonon-assisted indirect transitions between electrons in the four equivalent L valleys and holes located in a valence band Γ_v, in a neighborhood of the Γ point, is[17]

$$R_{ab/em}^{L_c\Gamma_v}(\hbar\omega) = \frac{e^2 n_1\omega|D_{\mathrm{eff}}|^2(2m^{*L_c})^{\frac{3}{2}}(n_{ph}+1/2\mp 1/2)|p^{\Gamma_{vc}}|^2}{12\pi^5\epsilon_0 m_0^2 c^3\rho\hbar^3\omega_{ph}} \int_0^{+\infty} d\epsilon^{L_c}\sqrt{\epsilon^{L_c}} f_e(E^{L_c}+\epsilon^{L_c}) \times \int_{-\infty}^{\infty} dk_\perp \int_0^{+\infty} k_\parallel dk_\parallel f_h\left(E_{\boldsymbol{k}}^{\Gamma_v}\right)\delta\left(E^{L_c}+\epsilon^{L_c}-E_{\boldsymbol{k}}^{\Gamma_v}-\hbar\omega\pm\hbar\omega_{ph}\right)\frac{1}{\left(E_{\boldsymbol{k}}^{\Gamma_c}-E^{L_c}-\epsilon^{L_c}\mp\hbar\omega_{ph}\right)^2}. \tag{12}$$

In the above expression, as specified by the ab/em index, the upper (lower) sign refers to the case of absorption (emission) of a phonon with energy $\hbar\omega$; D_{eff} is an effective deformation potential for the optical branch, ϵ^{L_c} represents the reduced electronic energy measured from the edge E^{L_c} of the L valley, and, as before, $f_{e,h}$ are the Fermi distributions. The energy cutoff related to the Fermi distribution in the conduction band suggests to approximate the denominator in the above equation $(E_{\boldsymbol{k}}^{\Gamma_c} - E^{L_c} - \epsilon^{L_c} \mp \hbar\omega_{ph})$ with the corresponding value calculated at $\boldsymbol{k}=0$. In this approximation one recovers the familiar

expression[17]

$$R^{L_c\Gamma_v}_{ab/em}(\hbar\omega) = \frac{2e^2 n_1 \omega |D_{\text{eff}}|^2 (m^{*L_c})^{\frac{3}{2}} (n_{ph} + 1/2 \mp 1/2) |p^{\Gamma_{vc}}|^2}{3\pi^6 \epsilon_0 m_0^2 c^3 \rho \hbar^6 \omega_{ph}} \frac{(m^{*\Gamma_v})^{\frac{3}{2}}}{(E^{\Gamma_c} - E^{L_c} \mp \hbar\omega_{ph})^2} \int_0^{\hbar\omega \mp \hbar\omega_{ph} - E^{L_c} + E^{\Gamma_v}} d\epsilon^{L_c} \times \sqrt{\epsilon^{L_c}} \sqrt{\hbar\omega \mp \hbar\omega_{ph} - \epsilon^{L_c} - E^{L_c} + E^{\Gamma_v}} f_e(E^{L_c} + \epsilon^{L_c}) f_h(E^{L_c} + \epsilon^{L_c} - \hbar\omega \pm \hbar\omega_{ph}), \tag{13}$$

where the valence density of states mass $m^{*\Gamma_v}$ is evaluated according to Eq. (6). On the other hand, for heavily doped n-type samples or for high temperatures, the above approximation becomes questionable. For this reason we report here also the exact expression for $R^{L_c\Gamma_v}_{ab/em}$ in Eq. (12) obtained after integration in $k_\parallel$,

$$R^{L_c\Gamma_v}_{ab/em}(\hbar\omega) = \frac{e^2 n_1 \omega |D_{\text{eff}}|^2 (2m^{*L_c})^{\frac{3}{2}} (n_{ph} + 1/2 \mp 1/2) |p^{\Gamma_{vc}}|^2 m_\parallel^{\Gamma_v}}{6\pi^5 \epsilon_0 m_0^2 c^3 \rho\, \omega_{ph} \hbar^5} \int_0^{+\infty} d\epsilon^{L_c} \sqrt{\epsilon^{L_c}} f_e(E^{L_c} + \epsilon^{L_c}) f_h(E^{L_c} + \epsilon^{L_c} - \hbar\omega \pm \hbar\omega_{ph}) \times \int_0^{k^{R_{\text{ind}}}_{ab/em}} \frac{dk_\perp}{\left[\left(1 + \frac{m_\parallel^{\Gamma_v}}{m^{\Gamma_c}}\right)(\mp\hbar\omega_{ph} - E^{L_c} - \epsilon^{L_c}) + E^{\Gamma_c} + \frac{m_\parallel^{\Gamma_v}}{m^{\Gamma_c}}(\hbar\omega + E^{\Gamma_v}) + \frac{\hbar^2 k_\perp^2}{2m^{\Gamma_c}}\left(1 - \frac{m_\parallel^{\Gamma_v}}{m_\perp^{\Gamma_v}}\right)\right]^2}, \tag{14}$$

where

$$k^{R_{\text{ind}}}_{ab/em} = \left[\frac{2m_\perp^{\Gamma_v}}{\hbar^2}(\hbar\omega \mp \hbar\omega_{ph} - E^{L_c} - \epsilon^{L_c} + E^{\Gamma_v})\right]^{\frac{1}{2}}. \tag{15}$$

Note that the integral in the $k_\perp$ variable of Eq. (14) can be evaluated analytically.

The total radiative recombination rate can be therefore written as

$$R = \sum_v R^{\Gamma_v} = \sum_v R^{\Gamma_c\Gamma_v} + R^{L_c\Gamma_v}_{ab} + R^{L_c\Gamma_v}_{em}, \tag{16}$$

where R^{Γ_v} is the recombination rate associated with transitions involving one of the HH, LH, or SO valence bands.

C. Optical absorption

The absorption coefficient due to the net balance of radiative transitions across the direct gap, $\alpha^{\Gamma_v\Gamma_c}_{\text{TE,TM}}$, is calculated as a function of the valence and conduction Fermi energies and for both TE and TM polarization versors from the expression[18]

$$\alpha^{\Gamma\Gamma_c}_{\text{TE,TM}}(\hbar\omega) = \frac{e^2}{2\pi n_1 c \varepsilon_0 m_0^2 \omega} \sum_v |\boldsymbol{p}^{\Gamma_{vc}} \cdot \hat{\boldsymbol{e}}_{\text{TE,TM}}|^2 \int_{-\infty}^{\infty} dk_\perp \int_0^{+\infty} k_\parallel dk_\parallel \delta\left(E^{\Gamma_c}_{\boldsymbol{k}} - E^{\Gamma_v}_{\boldsymbol{k}} - \hbar\omega\right)\left[1 - f_h\left(E^{\Gamma_v}_{\boldsymbol{k}}\right) - f_e\left(E^{\Gamma_c}_{\boldsymbol{k}}\right)\right], \tag{17}$$

where the sum considers the contributions from all three valence bands. After integration in $k_\parallel$ we find

$$\alpha^{\Gamma\Gamma_c}_{\text{TE,TM}}(\hbar\omega) = \frac{e^2}{\pi n_1 \varepsilon_0 m_0^2 \hbar^2 c\omega} \sum_v |\boldsymbol{p}^{\Gamma_v c} \cdot \hat{\boldsymbol{e}}_{\text{TE,TM}}|^2 m_\parallel^{\Gamma_{vc}} \int_0^{k^{\text{dir}}} dk_\perp \frac{1}{1 + e^{\frac{Ak_\perp^2 + B^v}{kT}}} - \frac{1}{1 + e^{\frac{Ak_\perp^2 + B^c}{kT}}}, \tag{18}$$

with k^{dir} defined in Eq. (11).

The indirect absorption coefficient contains contributions from absorption and stimulated photon-emission processes. In both cases transitions can be assisted by either absorption or emission of a phonon. Therefore, for each valence band Γ_v the evaluation of its contribution to the optical (net) absorption coefficient due to indirect transitions $\alpha^{\Gamma L}$ requires the distinction between processes involving photon absorption ($\Gamma_v \to L_c$) and photon-stimulated emission ($L_c \to \Gamma_v$) and between processes involving the emission (em) and absorption (ab) of an optical phonon:

$$\alpha^{\Gamma_v L_c} = \alpha^{\Gamma_v L_c}_{ab} + \alpha^{\Gamma_v L_c}_{em} - \alpha^{L_c\Gamma_v}_{ab} - \alpha^{L_c\Gamma_v}_{em}. \tag{19}$$

After summation over the valence bands, the photon absorption terms $\alpha^{\Gamma L_c}_{ab/em} = \sum_v \alpha^{\Gamma_v L_c}_{ab/em}$ are given by[18]

$$\alpha^{\Gamma L_c}_{ab/em}(\hbar\omega) = \frac{e^2 |D_{\text{eff}}|^2 (2m^{*L_c})^{\frac{3}{2}} (n_{ph} + 1/2 \mp 1/2)}{4\pi^3 n_1 \epsilon_0 m_0^2 c \rho \hbar^2 \omega\omega_{ph}} \sum_v |\boldsymbol{p}^{\Gamma_{vc}} \cdot \hat{\boldsymbol{e}}_{\text{TE,TM}}|^2 \int_0^{+\infty} d\epsilon^{L_c} \sqrt{\epsilon^{L_c}} [1 - f_e(E^{L_c} + \epsilon^{L_c})] \times \int_{-\infty}^{\infty} dk_\perp \int_0^{\infty} k_\parallel dk_\parallel \left[1 - f_h\left(E^{\Gamma_v}_{\boldsymbol{k}}\right)\right] \delta\left(E^{L_c} + \epsilon^{L_c} - E^{\Gamma_v}_{\boldsymbol{k}} - \hbar\omega \mp \hbar\omega_{ph}\right) \frac{1}{\left(E^{\Gamma_c}_{\boldsymbol{k}} - E^{L_c} - \epsilon^{L_c} \pm \hbar\omega_{ph}\right)^2}. \tag{20}$$

With the usual algebra we obtain

$$\alpha^{\Gamma L_c}_{ab/em}(\hbar\omega) = \frac{e^2|D_{\text{eff}}|^2(2m^{*L_c})^{\frac{3}{2}}(n_{ph}+1/2\mp 1/2)}{2\pi^3 n_1\epsilon_0 m_0^2 c\rho\hbar^4\omega\omega_{ph}}\sum_v |\boldsymbol{p}^{\Gamma_{vc}}\cdot\hat{\boldsymbol{e}}_{\text{TE,TM}}|^2 m_{\parallel}^{\Gamma_v}$$
$$\times\int_0^{+\infty} d\epsilon^{L_c}\sqrt{\epsilon^{L_c}}[1-f_e(E^{L_c}+\epsilon^{L_c})][1-f_h(E^{L_c}+\epsilon^{L_c}-\hbar\omega\mp\hbar\omega_{ph})]$$
$$\times\int_0^{k^{\alpha_{\text{ind}}}_{ab/em}}\frac{dk_\perp}{\left[\left(1+\frac{m_\parallel^{\Gamma_v}}{m^{\Gamma_c}}\right)(\pm\hbar\omega_{ph}-E^{L_c}-\epsilon^{L_c})+E^{\Gamma_c}+\frac{m_\parallel^{\Gamma_v}}{m^{\Gamma_c}}(\hbar\omega+E^{\Gamma_v})+\frac{\hbar^2k_\perp^2}{2m^{\Gamma_c}}\left(1-\frac{m_\parallel^{\Gamma_v}}{m_\perp^{\Gamma_v}}\right)\right]^2}, \tag{21}$$
$$k^{\alpha_{\text{ind}}}_{ab/em} = \left[\frac{2m_\perp^{\Gamma_v}}{\hbar^2}(\hbar\omega\pm\hbar\omega_{ph}-E^{L_c}-\epsilon^{L_c}+E^{\Gamma_v})\right]^{\frac{1}{2}}.$$

A similar equation holds for the stimulated photon emission term $\alpha^{L_c\Gamma}_{ab/em}$.

In tensile Ge-based light-emitting devices, a relevant contribution to the absorption coefficient comes from free carrier intraband absorption α^{fc}, owing to high n-type doping density and/or to the high density of injected excess carriers.[19] For these reasons we estimate the total absorption coefficient $\alpha_{\text{TE,TM}}$ as $\alpha^{bb}_{\text{TE,TM}}+\alpha^{fc}$, where $\alpha^{bb}_{\text{TE,TM}}$ is the interband contribution to the absorption coefficient which can be written for a given propagation direction and polarization mode as

$$\alpha^{bb}_{\text{TE,TM}} = \alpha^{\Gamma\Gamma_c}_{\text{TE,TM}}+\alpha^{\Gamma L_c}_{\text{TE,TM}}. \tag{22}$$

To quantify α^{fc}, we rely on the empirical relation reported by Liu *et al.* in Ref. 19, which describes the free carrier absorption of holes in the valence band and electrons in the conduction band, in terms of an empirical fit of measurements performed on p- and n-type Ge samples. For completeness, we explicitly report here the expression for α^{fc} proposed by Liu *et al.*:

$$\alpha^{fc}(\lambda) = 10^{-25}(3.2p\lambda^{2.43}+3.4n\lambda^{2.25}). \tag{23}$$

In the above equation $p=p_0+\delta p$ and $n=n_0+\delta n$ are the total (i.e., equilibrium plus excess) hole and electron densities expressed in cm^{-3}, λ is the photon wavelength in units of nm, and the resulting α^{fc} is expressed in cm^{-1}. We point out that the strain effect on the intervalence band absorption is not included in this formula. Notice that from the recent attempts to obtain optical gain in highly excited Ge samples, the free carrier absorption has emerged as the main obstacle to achieve an efficient laser action.[8,20] A precise evaluation of the losses due to α^{fc} in this condition is then crucial. Indeed, some discrepancies exist between results obtained by means of the above relation and very recent data measured by Carroll *et al.* in Ref. 20 (see, for instance, the critical discussion reported in Ref. 8). Nevertheless, at the present time Eq. (23) seems to properly describe, at least close to $T=300$ K, the majority of the experimental data as also suggested by Dutt and co-workers.[8]

III. RESULTS

The effect of the biaxial tensile strain on the band edges and energy gaps of [001]-oriented Ge films is summarized in Fig. 1. If we assume the band edge of the LH valence energy as reference zero energy (dotted line, independent of $\varepsilon_\parallel$), the energies of the L_c and Γ_c conduction edges are decreasing functions of the in-plane strain $\varepsilon_\parallel$. Since the conduction deformation potential for the Γ_c band is larger than the L-band one,[4,10] the Γ_c-L_c energy difference decreases with $\varepsilon_\parallel$. Starting from the unstrained value of $\Gamma_c-L_c=134$ meV (green solid curve in Fig. 1), the energy difference vanishes for $\varepsilon_\parallel\simeq 1.6\%$. This results in an indirect-to-direct band-gap crossover with a corresponding gap energy of 540 (600) meV at 300 (77) K. We notice (see Fig. 1) that while the values at room temperature of the direct (indirect) gap in the explored $\varepsilon_\parallel$ range is always about 80 and 70 meV lower than the corresponding values at 77 K, the Γ_c-L_c energy difference as function of the strain field is practically constant with temperature (not shown). We also point out that the tensile strain removes the HH-LH valence band degeneracy at the Γ point and lowers the HH band edge with respect to the LH band-edge energy. Therefore, while in relaxed Ge layers the large majority of holes is accommodated in the HH band because of its larger density of states, in tensile-strained Ge crystals, holes occupy

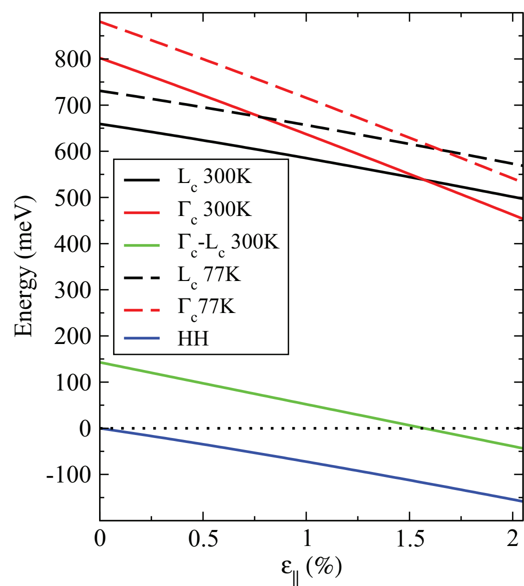

FIG. 1. (Color online) Band-edge energies in Ge as a function of the in-plane biaxial strain $\varepsilon_\parallel$ calculated with the topmost LH valence band set as reference zero energy. Solid and dashed black (red) curves represent the L_c (Γ_c) edges at 300 K and 77 K, respectively. The HH edge (blue) and the Γ_c-L_c energy difference at 300 K (green) are also shown.

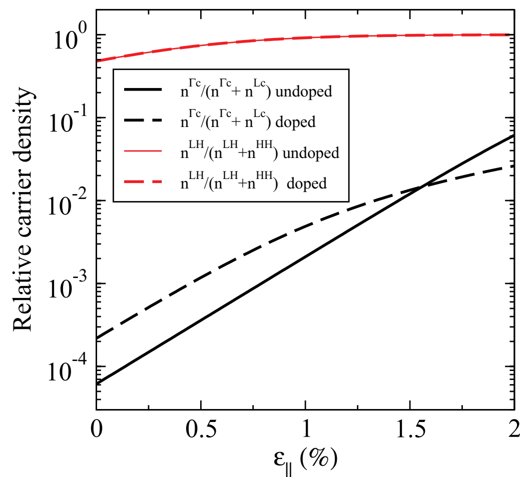

FIG. 2. (Color online) Relative carrier densities at 300 K calculated with an excess electron-hole carrier concentration $\delta n = 10^{18}$ cm^{-3} as function of the in-plane biaxial strain $\varepsilon_{\|}$ for undoped Ge (solid curves) and n-type Ge with doping density of 5×10^{19} cm^{-3} (dashed curves). The black (red) lines represent the carrier densities in the Γ_c (LH) valley, normalized to the total carrier density in the conduction (valence) band.

mainly the LH band. As we shall discuss in the following, the LH density-of-states mass $m^{*\mathrm{LH}}$ also increases with $\varepsilon_{\|}$, contributing to a further increase of the hole population in LH states.

The lowering of the $\Gamma_c - L_c$ energy difference in tensile-strained Ge causes a population redistribution of the conduction carriers towards the Γ_c states. This effect is shown in Fig. 2, where the L_c and Γ_c carrier densities are plotted as functions of $\varepsilon_{\|}$. The black lines in Fig. 2 represent the relative equilibrium plus excess carrier density $n^{\Gamma_c} = n_0^{\Gamma_c} + \delta n^{\Gamma_c}$ in the Γ_c valley, normalized to the total $n^{\Gamma_c} + n^{L_c}$ conduction carrier density. These quantities are evaluated at 300 K with an excess carrier density of $\delta n = 10^{18}$ cm^{-3} for undoped Ge (solid lines) and n-type doped Ge with doping density n_{dop} equal to 5×10^{19} cm^{-3} (dashed lines). We find that for undoped (doped) Ge the relative Γ_c electron density, n^{Γ_c}, increases from 6×10^{-5} (2×10^{-4}) to 6×10^{-2} (3×10^{-2}), when $\varepsilon_{\|}$ increases from zero to 2%. The corresponding absolute values for n^{Γ_c} (not shown) in undoped and doped Ge start from about 6×10^{13} and 1×10^{16} cm^{-3}, respectively, and at $\varepsilon_{\|} = 2\%$ reaches 7×10^{16} and 1×10^{18} cm^{-3}. Owing to the density of states associated with the fourfold degenerate L valleys, much larger than the Γ_c one, the large majority of electronic carriers remains in the L valleys also for strain values $\varepsilon_{\|} \gtrsim 1.6\%$, when the fundamental gap becomes direct. Moreover, we can observe from Fig. 2 that the relative population of the Γ_c valley in the indirect gap regime is larger for doped Ge than for intrinsic Ge; the opposite holds beyond the indirect-direct gap crossover. For holes, the above-discussed transfer of HH carriers into the LH band is practically identical in n-type intrinsic Ge (see red lines in Fig. 2). In our simulations, the fraction of LH carriers $n^{\mathrm{LH}} = n_0^{\mathrm{LH}} + \delta n^{\mathrm{LH}}$, normalized to the $n^{\mathrm{LH}} + n^{\mathrm{HH}}$ density, reaches the value of 90% at $\varepsilon_{\|} \simeq 0.96\%$; at $\varepsilon_{\|} \simeq 2\%$ less than 1% of the holes populate the HH band (the SO band always accommodates a negligible carrier density).

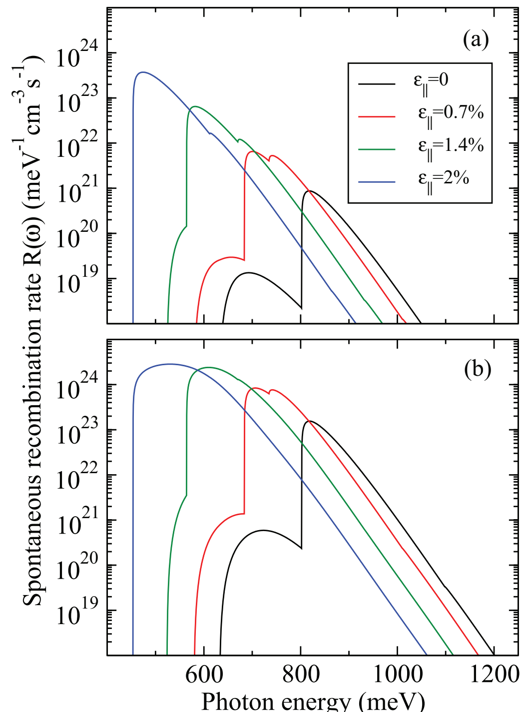

FIG. 3. (Color online) Spontaneous radiative recombination rate $R(\hbar\omega)$ as function of the emitted photon energy at 300 K calculated with an excess electron-hole carrier concentration $\delta n = 10^{18}$ cm^{-3} for different values of the in-plane biaxial strain. (a) Spectra for undoped Ge. (b) Spectra for n-type Ge with doping density of 5×10^{19} cm^{-3}.

The strain-induced carrier redistribution in the L_c and Γ_c conduction valleys greatly impacts the energy spectrum of the spontaneous recombination rate $R(\hbar\omega)$, as can be seen in Fig. 3, where we display the numerical data obtained at $T = 300$ K for undoped Ge (top panel) and n-type Ge with doping density $n_{\mathrm{dop}} = 5 \times 10^{19}$ cm^{-3} (bottom panel). For $\varepsilon \lesssim 1.4\%$ the two main features observed in the $R(\hbar\omega)$ spectra are related to the radiative recombination through the direct $\Gamma_c - \Gamma$ (higher energy peak) and phonon-assisted $L_c - \Gamma$ (lower energy peak) optical transitions. In agreement with the results shown in Fig. 1, we see that the direct and indirect peaks both redshift and get closer in energy for increasing $\varepsilon_{\|}$; they completely merge at $\varepsilon \sim 2\%$ (blue curves in Fig. 3). Note that for intermediate strain values in the direct gap energy region shown in Fig. 3 the signatures of the nondegenerate HH and LH bands are distinguishable, since in this regime both of them are populated. The most striking feature observable in Fig. 3 is the great enhancement of the recombination rate in tensile-strained Ge; it is clear that the increase of R is due to the enhancement of the $\Gamma_c - \Gamma$ peak, which, for the chosen excitation density and temperature, dominates the indirect recombination rate already at zero strain. This happens despite the fact that the large majority of electrons remains in the L valley, because the rate for the direct transitions is much larger than the indirect ones. As a consequence, a small variation of the L_c electron carrier density in favor of the Γ_c one causes a huge increase in the recombination rate. In agreement with the results of Fig. 2 the maximum for $R(\hbar\omega)$ is obtained for the doped system at

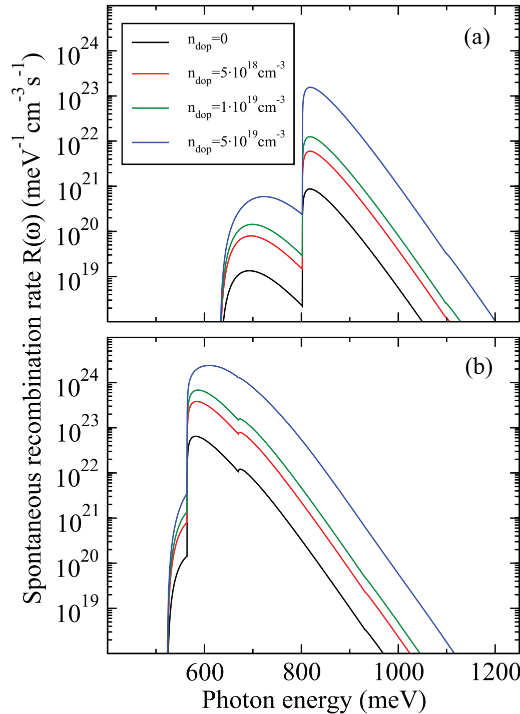

FIG. 4. (Color online) Spontaneous radiative recombination rate $R(\hbar\omega)$ as function of the emitted photon energy, at 300 K, calculated with an excess electron-hole carrier concentration $\delta n = 10^{18}$ cm^{-3} for different values of the n-type doping concentration. (a) Spectra for unstrained Ge. (b) Spectra for 1.4% tensile-strained Ge.

$\hbar\omega \simeq 550$ meV and $\varepsilon \sim 2\%$. On the other hand, the relative enhancement of $R(\hbar\omega)$ with the strain field is greater in the undoped material, where the recombination rate spans over three orders of magnitude as $\varepsilon_\parallel$ ranges in the 0%–2% interval.

To better clarify the role of doping, spontaneous recombination rate spectra have been calculated for different doping levels, as shown in Fig. 4, where we report the room-temperature values of $R(\hbar\omega)$ calculated for different n-type donor concentrations, in the case of unstrained Ge (top panel) and 1.4% tensile-strained Ge (bottom panel). As one can expect, a dopant density increase at a constant excess of carrier density ($\delta n = 10^{18}$ cm^{-3}) entails larger recombination rates related to both direct and phonon-assisted radiative transitions. This fact is due to the increase of conduction electrons available for recombination processes. We find that the total (excess plus equilibrium) conduction carrier densities in the L_c and Γ_c valleys increase with doping in a very different extent. In fact, most of the donor electrons always lie in the L valleys, due to the lower energy and larger density of states. For the unstrained (strained) Ge system, the ratio between the Γ_c and L_c electron densities varies from 6×10^{-5} to 2×10^{-4} (9×10^{-3} to 1×10^{-2}) when the doping density increases from zero to 5×10^{19} cm^{-3}. On the other hand, in line with the above considerations, we observe that the most relevant changes in the recombination rates concern the peak associated with the direct transitions, which reaches in the relaxed and in the strained Ge material the values 1.5×10^{23} and 2×10^{24} meV^{-1} cm^{-3} s^{-1}, respectively. In relative terms, we find that when increasing the doping density up to 5×10^{19} cm^{-3}, the contribution to $R(\hbar\omega)$ originating from the direct transitions is enhanced in the relaxed (strained) Ge by a factor of 200 (30) while for the contribution to $R(\hbar\omega)$ due to the indirect transitions we evaluate a corresponding enhancement factor of 60 (50).

Figure 5 summarizes the main results discussed insofar, offering an overall view of the dependence of the recombination rate on the strain field intensity and on the doping concentration. The contour plot in the left panel of Fig. 5 represents the maximum of the $R(\hbar\omega)$ spectrum, calculated at $T = 300$ K with $\delta n = 10^{18}$ cm^{-3}, as function of $\varepsilon_\parallel$ and $n_{\rm dop}$. In line with the above results, we find that the maximum intensity of the recombination spectrum $R(\hbar\omega)$ is always associated to the direct transitions. Its value is a monotonically increasing function of both $\varepsilon_\parallel$ and $n_{\rm dop}$ spanning three orders of magnitude in the ($\varepsilon_\parallel$, $n_{\rm dop}$) parameter space explored in Fig. 5. In the left panel of Fig. 5 it is apparent that a kink in the shape of the isolines is present. This behavior is clarified with the help of the right plot of Fig. 5, where we show in the ($\varepsilon_\parallel$,$n_{\rm dop}$) plane the photon energy at which the maximum of the $R(\hbar\omega)$ spectrum occurs. In the low-strain region the spectral maximum of $R(\hbar\omega)$ is associated with the direct transitions involving the HH band that indeed hosts the majority of valence carriers. When the strain is increased, carriers start to populate mainly the LH band, since it is located at lower hole energy. As a consequence the maximum of $R(\hbar\omega)$ is now related to radiative recombinations involving this latter valence band. It follows that at the crossover between the HH and LH "regimes" (which depends on both $\varepsilon_\parallel$ and $n_{\rm dop}$), we can observe a discontinuity

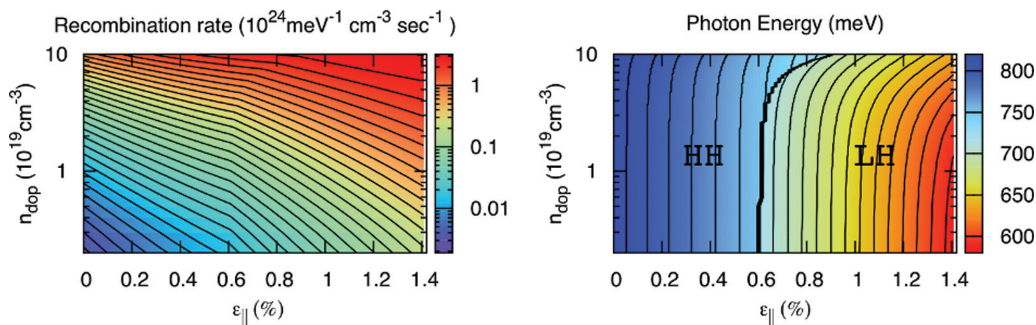

FIG. 5. (Color online) Maximum of the spontaneous radiative recombination rate $R(\hbar\omega)$ spectrum (left) and related photon energy (right), calculated at 300 K as functions of the in-plane biaxial strain $\varepsilon_\parallel$ (horizontal axis) and of the n-type doping concentration (vertical axis) with an excess electron-hole carrier concentration $\delta n = 1 \times 10^{18}$ cm^{-3}.

in the photon energy at which the $R(\hbar\omega)$ spectrum peak is present. It is interesting to notice that the isolines plotted in the right panel of Fig. 5 are not vertical, despite the fact that our model neglects the dependency of band edges on the doping concentration. The bending of the isolines toward higher values of $\varepsilon_\parallel$ observed in the upper part of the $(\varepsilon_\parallel, n_{\rm dop})$ plane is a signature of the conduction band filling, occurring at high doping densities. This filling activates radiative transitions occurring at energies higher than those involving carriers at the conduction band edge: For a given $\varepsilon_\parallel$ value the $R(\hbar\omega)$ peak blueshifts increasing $n_{\rm dop}$.

Our modeling results can be used to understand better the observed behavior of the photoluminescence (PL) from Ge films as a function of the lattice temperature. As a matter of fact, it has been reported[21] that the PL intensity measured in Ge thin films at different temperatures and constant optical pump power increases for higher T. This very peculiar behavior of the PL spectrum is related to the quasidirect nature of Ge and can be interpreted in terms of conduction carrier redistribution, induced by thermal activation, from the L_c into the Γ_c valley: The radiative recombination rate increases with T because of the activation of the direct transitions. In this way, despite the reduction of the photoexcited valence and conduction carrier densities, caused by the enhancement of the nonradiative recombination channels, the PL signal becomes more intense due to the greater radiative recombination rate associated to the activated direct transitions. This behavior is in agreement with the results reported in Fig. 6, where we show the $R(\hbar\omega)$ spectra, calculated at different lattice temperatures using a constant excess carrier density $\delta n = 10^{18}$ cm^{-3}. In the case of intrinsic (top panel) and 5×10^{19} cm^{-3} n-doped (central panel) relaxed Ge we find qualitatively similar behaviors. At low temperature the L_c-Γ transitions dominate the spectrum since a negligible amount of conduction carriers lies in the Γ valley. Upon increasing the lattice temperature from 77 K to 300 K, the direct gap-related contribution to the spectrum increases dramatically, covering almost seven and four orders of magnitude in the intrinsic and the doped systems, respectively. We point out here again that this behavior is driven by the transfer of a very tiny fraction of the L_c carriers into the Γ_c valley (i.e., 6×10^{-5} and 1×10^{-2} at 300 K in the intrinsic and doped system, respectively), as one can argue by the very moderate decrease of the indirect transition-related feature shown in Figs. 6(a) and 6(b). The $R(\hbar\omega)$ spectrum of $\varepsilon_\parallel = 1.4\%$ tensile Ge behaves differently, as shown in the bottom panel of Fig. 6, where we can observe much smaller temperature-induced spectral changes. In fact, the direct transition signal dominates the indirect one already at low temperature and when T increases up to 300 K, its intensity varies less than 50%. This fact can be understood noticing that at this strain value, the energy difference between the L_c and Γ_c conduction band edges is quite low (about 12 and 20 meV at 77 K and 300 K, respectively). It follows that the relative variation induced by the temperature in the Γ_c carrier density is not as relevant as in the case of relaxed Ge. For instance, in the doped system of Figs. 6(b) the Γ density ranges from 4×10^{11} to 1×10^{16} cm^{-3}, when T varies in the 77 K–300 K interval while in the strained material [Fig. 6(c)] the carrier density in the Γ valley increases only one order of magnitude, from the 77 K value of 8×10^{14} to the value 9×10^{15} cm^{-3} at 300 K. The main effect in the latter case is the thermal broadening of the direct transition peak, while the maximum of R is only slightly changed. As a final comment to Fig. 6(c) we underline the presence of features related to the HH band edge, whose hole population is an increasing function of T.

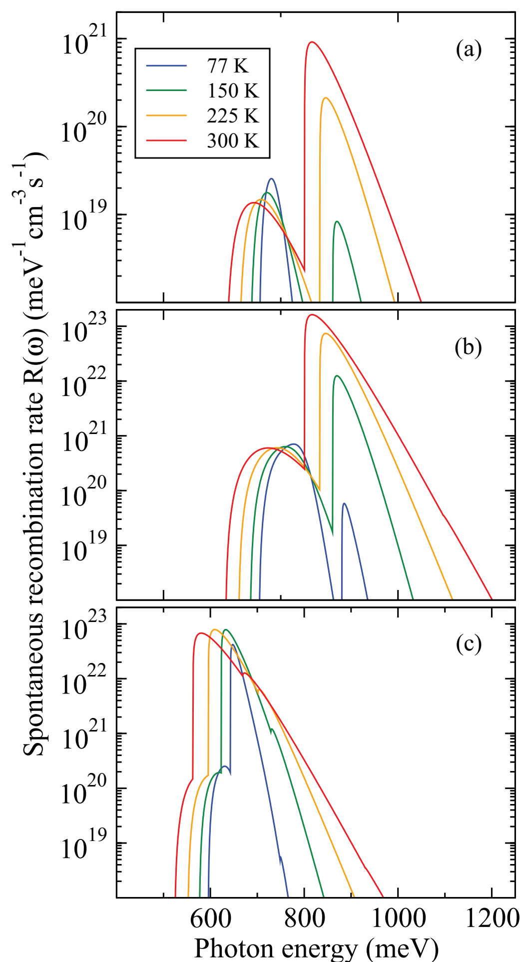

FIG. 6. (Color online) Spontaneous radiative recombination rate $R(\hbar\omega)$ as function of the emitted photon energy calculated with an excess electron-hole carrier concentration $\delta n = 10^{18}$ cm^{-3} for different temperature values. Spectra for unstrained intrinsic Ge (top), for unstrained n-type Ge with doping density of 5×10^{19} cm^{-3} (middle), and for 1.4% tensile-strained intrinsic Ge (bottom), are shown.

We now discuss the results obtained on the absorption/gain coefficient, which we have studied as a function of the strain and doping concentration, for different excitation levels. Our main findings are summarized in the contour plots of Fig. 7, where in the $(\varepsilon_\parallel, n_{\rm dop})$ plane the minimum value of the $\alpha(\hbar\omega) = \alpha^{bb}(\hbar\omega) + \alpha^{fc}(\hbar\omega)$ spectrum is reported. Numerical data in Fig. 7 have been obtained at $T = 300$ K and in the top, center, and bottom panels δn is equal to 1×10^{18}, 5×10^{18}, and 1×10^{19} cm^{-3}, respectively. Left- and right-column panels refer to the case of polarization vector parallel (TE mode) and orthogonal (TM mode) to the growth plane, respectively. Except for the low excitation density regime in the TE mode (top-left panel), a positive gain region in the $(\varepsilon_\parallel, n_{\rm dop})$ plane, i.e., negative absorption coefficient, is present in each plot of Fig. 7. The boundaries of such regions are identified by

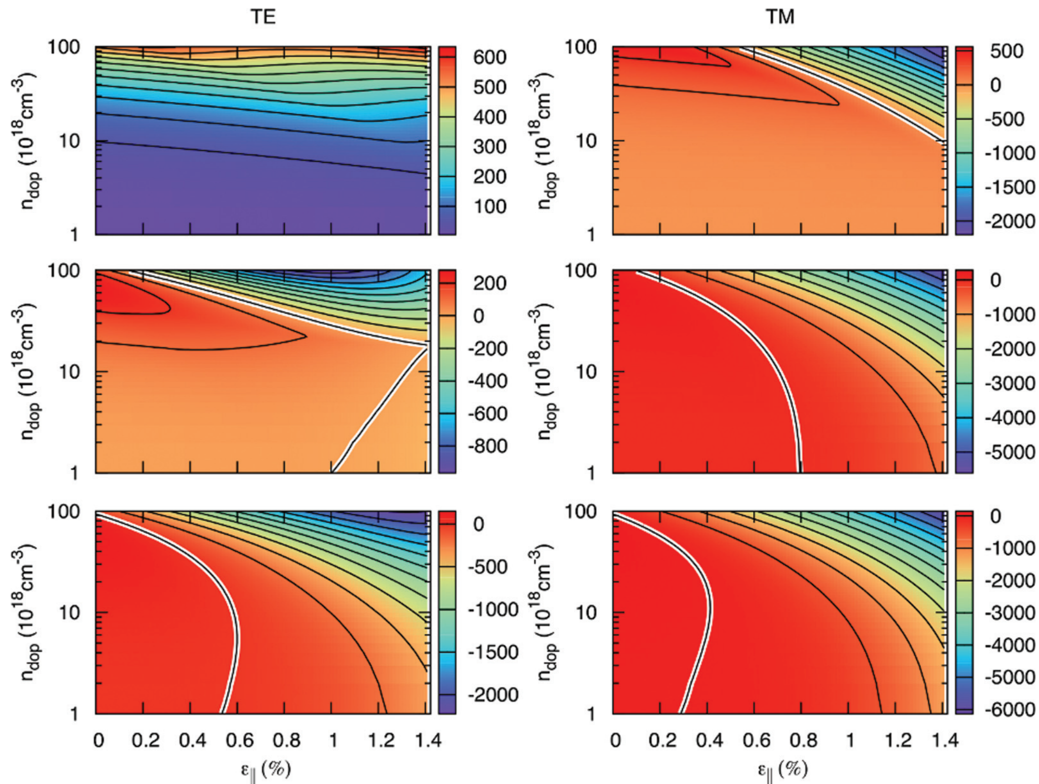

FIG. 7. (Color online) Minimum of the total (band-to-band and free-carrier contributions) absorption coefficient spectrum $\alpha(\hbar\omega)$ in cm^{-1}, calculated at 300 K as functions of the in-plane biaxial strain $\varepsilon_{\parallel}$ (horizontal axis) and the n-type doping concentration (vertical axis). In the top, middle, and bottom panels, the excess electron-hole carrier concentrations δn are equal to 1×10^{18}, 5×10^{18}, and 1×10^{19} cm^{-3}, respectively. Left (right) column plots are obtained with the polarization vector parallel (orthogonal to) the growth plane. When present, the isoline corresponding to the transparency condition is marked in white.

the $\alpha = 0$ transparency isolines, which have been marked in white. The predicted positive gain values can be quite robust, especially in the high-strain, high-doping parameter region. For instance, at $\varepsilon_{\parallel} = 1.4\%$ and $n_{\mathrm{dop}} = 1 \times 10^{20}$ cm^{-3}, we obtain for $\delta n = 1 \times 10^{19}$ cm^{-3} a gain coefficient in the TE and TM mode of about 2×10^3 and 5×10^3 cm^{-1}, respectively. Note that for given excess carrier density the largest gain coefficients are always found in the TM mode. In fact, for high values of the strain field the active radiative recombinations involve the LH band and in this case the associated oscillator strength is maximized when the polarization vector is orthogonal to the growth plane. In the high-strain, high-doping parameter region the gain generally increases with both $\varepsilon_{\parallel}$ and n_{dop}. We notice, however, that a qualitatively different dependence on the strain and doping levels can be obtained, as it happens, for instance, for the configuration corresponding to the left-central panel. Indeed, in this case the gain has a maximum at $n_{\mathrm{dop}} = 1 \times 10^{20}$ cm^{-3} and $\varepsilon_{\parallel} = 1\%$, i.e., before the strain boundary value of 1.4%. This fact can be interpreted considering the strain dependence of the square modulus of the dipole matrix element, which we have evaluated by means of the tight-binding model. For the Γ_c-LH transition in the TE mode we have found that the dipole element is a decreasing function of the strain intensity while the strain dependence of the dipole matrix element related to the Γ_c-HH recombination turns out to be much weaker in both TE and TM polarization. It follows that the interplay between the increasing of the Γ_c carrier density controlled by $\varepsilon_{\parallel}$ and the accompanying decrease of the Γ_c-LH oscillator strength results in a gain peak located before the boundary value of 1.4%. On the other hand, since our tight-binding calculations indicate that in the TM mode the square modulus of the dipole matrix element for the Γ_c-LH recombination increases with the strain intensity, the TM gain remains a monotonic function of $\varepsilon_{\parallel}$. Consequently, at low excitation density ($\delta n = 1 \times 10^{18}$ cm^{-3}, top panels) positive gain is obtained only for TM polarization in the high-strain, high-doping range; in the same parameter range the TE polarized absorption remains positive, being dominated by the free carrier losses. It is apparent from Fig. 7 that to obtain high positive gain heavy doping is not a mandatory requirement if high tensile strain values can be achieved. As an example we consider the case of $\delta n = 5 \times 10^{18}$ cm^{-3} in the TM mode. The same gain value of about 500 cm^{-1} is predicted for the case of heavy doping (1×10^{20} cm^{-3}) and moderate strain field (0.3%) and the case of light doping (1×10^{18} cm^{-3}) and large strain field (1.4%). Of course, the photon energy at which the gain is maximum is not the same, being lower when the strain is larger. This feature expands the design possibility of optoelectronic devices based on Ge and operating at different frequencies. Given a desired gain/absorption, one can design an active/passive device operating in a broad range of light wavelength. It is worth reminding the reader here that[22] the spectral window suitable for waveguiding in a Si photonic platform extends towards a wavelength of 3.5 μm (354 meV).

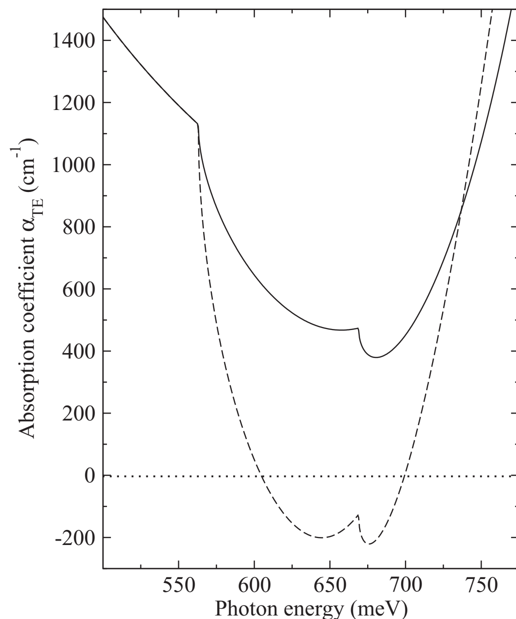

FIG. 8. Total (band-to-band and free-carrier contributions) absorption coefficient spectrum $\alpha(\hbar\omega)$, calculated at 300 K in TE mode for 1.4% tensile-strained n-type Ge with doping density of 1×10^{20} cm^{-3}. The excess electron-hole carrier concentration δn is equal to 2×10^{18}. The solid (dashed line) curve represents results obtained considering (neglecting) the dependence of the effective masses in the valence band and the dipole matrix elements on the strain field; accordingly, cylindrical (spherical) symmetry approximations for the effective masses in the valence band are assumed.

As a final remark we want to underline here that not only the band-edge modifications induced by the strain, but also the dependence of the density-of-states masses and of the dipole matrix elements on the strain field, must be taken into account in the calculation of the gain coefficient in strained Ge. To support this statement, in Fig. 8 we compare the room-temperature TE absorption spectrum of 1.4% strained n-type Ge, calculated considering the dependence of valence effective masses and dipole matrix elements from the strain, with the same spectrum obtained neglecting these effects, i.e., when the strain influences only the band edges. In Fig. 8 doping density and excess electron-hole carrier concentration has been set at 1×10^{20} and 2×10^{18} cm^{-3}, respectively. We see that the model in which the strain field influences only the band edges predicts a positive gain of about 200 cm^{-1}, while no gain is obtained if all the strain effects are properly considered. Indeed, the absorption coefficient remains positive, being dominated by the free carrier losses, mainly because the oscillator strength in the TE mode, associated with the Γ_c-LH transition, diminishes increasing $\varepsilon_\parallel$. We believe that this effect can account, at least partially, for the discrepancy observed between calculated and measured gain values in tensile-strained Ge layers.

IV. CONCLUSIONS

In this paper we have calculated the optical properties of bulk Ge as a function of tensile strain, doping, lattice temperature, and charge injection density. The full near-infrared spectrum of the recombination and gain coefficient has been calculated from the Fermi golden rule, taking into account direct and phonon-assisted transitions. Our calculations demonstrate that full quantum statistics for both carrier and lattice vibrations, as well as the consideration of strain effects on band curvature and on the dipole matrix elements, are essential to properly describe the optical properties of strongly excited and/or highly strained Ge samples. Our calculations confirm that increasing strain decreases the $\Gamma_c - L_c$ energy difference, leading to a crossover of the conduction band edges and therefore to a direct band gap structure, for $\varepsilon_\parallel \geqslant 1.6\%$. Consequently, tensile strain favors (also in the indirect gap regime) an electron redistribution towards the Γ_c valley. A relatively small carrier transfer from the L_c to the Γ_c valley is observed to induce a huge spontaneous recombination rate increase thanks to the much larger efficiency of the direct optical recombination $\Gamma_c \rightarrow \Gamma_v$, with respect to the indirect one $L_c \rightarrow \Gamma_v$. In strained structures, the peak of the spontaneous recombination spectrum $R(\hbar\omega)$ is dominated at all temperatures by the contribution of direct transitions occurring between Γ_c conduction states and HH valence states, for $\varepsilon_\parallel \leqslant 0.6\%$, or between Γ_c and LH states for larger values of biaxial strain. Its intensity is a monotonically increasing function of both strain and doping values. Net optical gain has also been computed for the values of strain (0%–1.4%) and doping (10^{18}–10^{20} cm^{-3}) here investigated. To account properly for the orbital symmetry of the valence and conduction band states involved in the transition, TE and TM light polarizations have been separately considered in the evaluation of the gain spectra. For selected and experimentally achievable doping and strain values, net optical gain values as high as 6000 cm^{-1} are predicted.

*virgilio@df.unipi.it

[1]T. Baehr-Jones, T. Pinguet, P. Lo Guo-Qiang, S. Danziger, D. Prather, and M. Hochberg, Nat. Photon. **6**, 206 (2012).

[2]W. Bogaerts, S. Selvaraja, P. Dumon, J. Brouckaert, K. De Vos, D. Van Thourhout, and R. Baets, IEEE J. Sel. Topics Quantum Electron. **16**, 33 (2010).

[3]G. Masini, S. Sahni, G. Capellini, J. Witzens, and C. Gunn, Adv. Opt. Technol. **2008**, 196572 (2008).

[4]J. Liu, D. D. Cannon, K. Wada, Y. Ishikawa, D. T. Danielson, S. Jongthammanurak, J. Michel, and L. C. Kimerling, Phys. Rev. B **70**, 155309 (2004).

[5]J. Liu, X. Sun, R. Camacho-Aguilera, L. C. Kimerling, and J. Michel, Opt. Lett. **35**, 679 (2010).

[6]D. Liang and J. Bowers, Nat. Photon. **4**, 511 (2010).

[7]R. E. Camacho-Aguilera, Y. Cai, N. Patel, J. T. Bessette, M. Romagnoli, L. C. Kimerling, and J. Michel, Opt. Express **20**, 11316 (2012).

[8]B. Dutt, D. Sukhdeo, D. Nam, B. Vulovic, Z. Yuan, and K. Saraswat, IEEE Photon. J. **4**, 2002 (2012).
[9]G. Capellini, G. Kozlowski, Y. Yamamoto, M. Lisker, C. Wenger, G. Niu, P. Zaumseil, B. Tillack, A. Ghrib, M. de Kersauson, M. E. Kurdi, P. Boucaud, and T. Schroeder, J. Appl. Phys. **113**, 013513 (2013).
[10]C. G. Van de Walle and R. M. Martin, Phys. Rev. B **34**, 5621 (1986).
[11]Y. P. Varshni, Physica (Utrecht) **34**, 149 (1967).
[12]C. D. Thurmond, J. Electrochem. Soc. **122**, 1133 (1975).
[13]Calvin Yi-Ping Chao and S. L. Chuang, Phys. Rev. B **46**, 4110 (1992).
[14]M. M. Rieger and P. Vogl, Phys. Rev. B **48**, 14276 (1993).
[15]M. Virgilio and G. Grosso, Phys. Rev. B **79**, 165310 (2009).
[16]Y. Busby, M. De Seta, G. Capellini, F. Evangelisti, M. Ortolani, M. Virgilio, G. Grosso, G. Pizzi, P. Calvani, S. Lupi, M. Nardone, G. Nicotra, and C. Spinella, Phys. Rev. B **82**, 205317 (2010).
[17]H. Bebb and E. Williams, in *Transport and Optical Phenomena*, Semiconductors and Semimetals Vol. 8, edited by R. Willardson and A. C. Beer (Elsevier, Amsterdam, 1972) Chap. 4, pp. 181–320.
[18]F. Bassani and G. Pastori Parravicini, *Electronic States and Optical Transitions in Solids* (Pergamon, Moscow, 1975).
[19]J. Liu, X. Sun, D. Pan, X. Wang, L. C. Kimerling, T. L. Koch, and J. Michel, Opt. Express **15**, 11272 (2007).
[20]L. Carroll, P. Friedli, S. Neuenschwander, H. Sigg, S. Cecchi, F. Isa, D. Chrastina, G. Isella, Y. Fedoryshyn, and J. Faist, Phys. Rev. Lett. **109**, 057402 (2012).
[21]T.-H. Cheng, C.-Y. Ko, C.-Y. Chen, K.-L. Peng, G.-L. Luo, C. W. Liu, and H.-H. Tseng, Appl. Phys. Lett. **96**, 091105 (2010).
[22]R. Soref, Nat. Photon **4**, 495 (2010).
[23]O. Madelung (editor), *Semiconductors: Group IV Elements and III-V Compounds* (Springer, New York, 1991).
[24]E. O. Kane, J. Phys. Chem. Solids **1**, 82 (1956).
[25]C. Jacoboni, F. Nava, C. Canali, and G. Ottaviani, Phys. Rev. B **24**, 1014 (1981).
[26]J.-M. Jancu and P. Voisin, Phys. Rev. B **76**, 115202 (2007).